Doped TiO2 aerogels as alternative catalyst supports for proton exchange membrane fuel cells: A comparative study of Nb, V and Ta dopants

Christian Beauger, Laetitia Testut, Sandrine Berthon-Fabry, Frédéric Georgi, Laure Guétaz

Doped TiO_2 aerogels as alternative catalyst supports for Proton Exchange Membrane Fuel Cells: a comparative study of Nb, V and Ta dopants.

C. Beauger*[1], L. Testut[1], S. Berthon-Fabry[1], F. Georgi[2] and L. Guetaz[3, 4]

1 MINES ParisTech, PSL Research University PERSEE - Centre procédés, énergies renouvelables et systèmes énergétiques, CS 10207 rue Claude Daunesse 06904 Sophia Antipolis Cedex, France

2 MINES ParisTech, PSL Research University CEMEF - Centre de Mise en Forme des Matériaux, UMR CNRS 7635, CS 10207, rue Claude Daunesse, 06904 Sophia Antipolis Cedex, France

3 University Grenoble Alpes, Grenoble F-38000, France

4 CEA, LITEN, 17 rue des martyrs , F-38054 Grenoble, France

* *Corresponding author*

Keywords: Doped Titania Aerogel, Morphology, Conductivity

Abstract

Nb, Ta and V-doped TiO_2 aerogels and xerogels have been synthesized as possible new alternatives to carbon blacks for Proton Exchange Membrane Fuel Cells catalyst supports. A comparative study of different dopants was realized in a single study. Nb, Ta and V showed different behaviors with respect to the final material structure and morphology, composition and electronic conductivity. They are all prone to surface segregation, to different extents. V-doped TiO_2 apart, the rutile structure could only be obtained after calcination in a reducing atmosphere at 800 °C for Nb or Ta-doped TiO_2. The electronic conductivity exhibited a maximum at 10 at.% for Nb and Ta, 5 at.% for V. Nb revealed to be the most appropriate dopant to increase the electronic conductivity of TiO_2, followed by Ta and V. 4 to 5 orders of magnitude were gained after Nb doping for xerogels conductivity to reach almost 0.1 S cm^{-1}. The role of point defects was discussed to account for phase transition and evolution of conductivity.

Graphical abstract

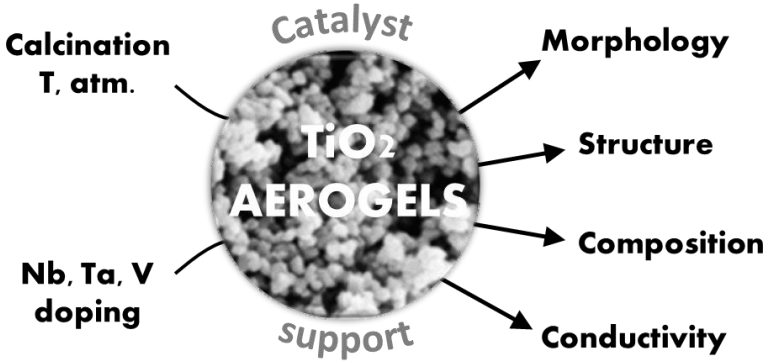

Introduction

Despite the recent commercialization of fuel cell cars in Japan, the mass development of proton exchange membrane fuel cells (PEMFC) for automotive application is still facing two main challenges: durability and cost. Both of them are interconnected and highly related to materials used in membrane electrodes assemblies (MEA), the unit cells where electrochemical reactions convert hydrogen and oxygen into electricity, heat and water. Among the components of MEAs, the catalyst layer is one of the main sources of durability and cost reduction. Due to its limited stability in PEMFC operating conditions [1, 2], numerous studies are dedicated to replacing carbon as catalyst support. Indeed, carbon tends to corrode under operation, especially at the cathode side [3, 4] due to high relative humidity associated to relatively high temperature (80 °C) and high potential (1.4 V in some operation phases like start-up/shut-downs [5]). Such corrosion would even be emphasized at higher operating temperature, a trend in PEMFC development. On one hand, carbon corrosion is responsible for a change in morphology of the catalyst layer with consequences on gas diffusion inside the electrodes. On the other hand, it is also impacting the supported catalyst whose particles number and repartition and size distribution are modified, resulting from particles aggregation, migration or detachment [6, 7], thus lowering the catalytic activity.

Different strategies have been followed to mitigate carbon corrosion, based either on system countermeasures or on new materials development. Among the several alternatives proposed to replace carbon as a catalyst support, metal oxides look promising. Stable metal oxides in PEMFC cathodic operating condition can be selected from Pourbaix (pH-potential) diagrams [8]. TiO_2 is one of

them. It is cheap and has been studied for long, especially for application in solar cells [9, 10] or for its photocatalytic properties [11, 12]. Different morphologies have thus already been developed, nanoparticles, nanotubes or even aerogels [13-23] for instance. Morphology is a major feature of PEMFC catalyst supports, especially at the cathode side, since it governs diffusion limitations related to gas diffusion towards (oxygen) and from (water) catalytic sites inside the cathodic catalyst layer.

To be considered as a potential alternative to carbon blacks, on top of having an adequate morphology, the electronic conductivity of TiO_2 has to be significantly increased. The electronic conductivity is related to the concentration of positively charged defects in the lattice. Hence doping TiO_2 with cations of higher valence than that of Ti (4+) or heating TiO_2 in a reducing atmosphere to favor the presence of oxygen vacancies will increase its electronic conductivity through charge compensation phenomenon. Both strategies have already been followed and conductivity as high as 1 S cm^{-1} has been reached [24], noteworthy most of the time at the expense of the specific surface area. Different cations such as Nb, V or Ta [24-30] have already been used as dopant in TiO_2.

Combining proper morphology (high specific surface area and adequate pore size distribution) and high electronic conductivity is mandatory for a material to be a credible alternative to carbon blacks as PEMFC catalyst support. Nanoparticles [25, 31, 32], nanotubes, microspheres [33, 34] or nanofibers [35] have been evaluated as different TiO_2 morphologies to replace carbon black as promising catalyst support for PEMFC. To our knowledge, despite their very interesting morphology, TiO_2 aerogels have never been evaluated in such an application. The potential of carbon aerogels in this area has already been demonstrated [36, 37]. With large specific surface area (650 m^2 g^{-1}) and a pore size distribution which can be tailored from the synthesis route parameters, they offer a wide panel of possible morphologies. Following our previous work on carbon aerogels for PEMFC [38, 39] and TiO_2 aerogels for water splitting [22], it came out obvious to try to design mesoporous TiO_2 for PEMFC. To this end we had to increase their electronic conductivity to reach values close to that of carbon (several S cm^{-1} depending on the material and the measurement technique). Considering that the trend in PEMFC is to increase the operating temperature and that the electronic conductivity of

semiconducting metal oxides is increasing with temperature alleviates somehow the constraint on the conductivity target.

For the first time in a single study, Nb, V or Ta-doped TiO_2 materials have been synthesized in the scope of reaching both adequate morphology and electronic conductivity for PEMFC. It is well known that the aerogel texture is highly impacted by the preparation route [40]. All synthesis parameters have thus to be optimized to reach the objectives. This study is focused on conditions of calcination (atmosphere and temperature) and type of dopant and their concentration. All these parameters have mutual influence and a whole study appeared necessary to optimize the material for the foreseen application. The results presented here report the influence of the synthesis parameters on the crystallographic structure, the specific surface area and pore size distribution, the chemical composition and the electronic conductivity of Nb, V or Ta-doped TiO_2 aerogels/xerogels.

2. Experimental

2.1 Synthesis route

Aerogels and xerogels were synthesized starting from a classical sol-gel route based on alkoxides [20] and already experienced in a previous study [22]. The following parameters have been selected for the whole study: R = H_2O/Ti = 3.4, C = HNO_3/Ti = 0.07 and S = iPrOH/Ti = 15.

All chemicals were purchased from Alfa Aesar and dried out on molecular sieve (HNO_3 2N ref.44528, $Ti(OBu)_4$ ref.77124, $Nb(OiPr)_4$ 99% 10%w/v in iPrOH (ref. 36572), $VO(iPrO)_3$ 96% (ref. 89798), Ta(OEt)5, 99+%, (ref.L10288).

Crystallized materials are obtained by calcination in a tubular furnace, 5 h at different temperatures (ramp of 10°C/min) in controlled atmosphere (air or 5 vol.% H_2 in N_2 hereafter mentioned H_2/N_2).

The nomenclature chosen to name the materials (ex. A8TN100) relates to their composition and conditions of preparation. The first letter stands for the type of materials (A for Aerogels, X for Xerogel). The first figure represents the temperature of calcination (8 for 800°C…). H is preceding the letter for samples calcined in H_2/N_2 (others are calcined in air). The following letter stands for the

matrix (T for TiO_2). And the end is mentioned the dopant (N for Nb, V for V, Ta for Ta) and its concentration level (100 for 10 at.%...). AH8TN100 stands for a 10 at .% Nb-doped TiO_2 aerogel calcined in H_2/N_2 at 800°C whereas XTN100 stands for its xerogel counterpart calcined in air.

2.2 Material characterization

X-ray diffraction (XRD) patterns were collected using a powder diffractometer (MPD PANalytical X'Pert Pro) operated at 45 kV, with CuKα radiation (λ= 0.154 nm). Data were collected in steps of 0.05 ° from 20° to 90 ° in 2-θ mode with Pixcel counter.

The X-ray photoelectron spectroscopy (XPS) analyses were carried out using a Thermo Scientific K-Alpha system. The spectrometer is equipped with an AlKα monochromated source and a low energy flood-gun for charge compensation. Survey scans were made with energy pass of 200 eV - step 1eV and high resolution analyses with pass energy 40 eV - step 0.1 eV. The ellipsoid spot size is about 350 µm x 700 µm. The thickness of analysis is about 10 nm with more than 80% of the signal coming from the first 5 nm.

Scanning electron microscopy (SEM) observations were recorded with a ZEISS Supra 40 with a 30 kV electron beam. The composition has been analyzed by energy dispersive X-ray spectroscopy (EDX) at 15 kV, performed with a Philips XL30. EDX and XPS analysis were repeated four times on the same sample.

Transmission electron microscopy (TEM) analyses in high resolution TEM (HRTEM) mode and in scanning TEM (STEM) mode have been performed using a FEI-Tecnai Osiris operating at 200 kV. This microscope is equipped with a Super-X system (4 Silicon Drift Detectors) optimized for high speed EDX elemental maps acquisition. The quantitative analysis of Ti and Nb composition was performed using the Ti and Nb K lines using Cliff-Lorimer k factors given by the EDX Bruker program.

Nitrogen sorption analysis was performed with a Micromeritics ASAP 2020. Samples were preliminary degassed during 120 min at 10 µmHg and 100 °C. Brunauer-Emmett-Taller (BET) model was applied to determine the specific surface area. The pore size distributions were calculated

applying the Barret-Joyner-Halenda (BJH) method to the desorption branch of the isotherms. The assessments of microporosity were made from t-plot construction using the Harkins-Jura correlation.

By considering a monomodal distribution of spherical particles, the mean particle diameter has been calculated applying the formula $d=6/(\rho S)$ (where d is the particle diameter, ρ the skeleton density = 4.26 g cm^{-3} [41] and S the specific surface area).

The "bulk" electronic conductivity was measured by electro-impedance spectroscopy (EIS) on doped xerogel pellets (13 mm in diameter), pressed during 5 min at 3.5 tons (CARVER) and calcined under hydrogen flux (H_2/N_2) at 800 °C during 5 hours. The conductivity (σ) was calculated with the formula $\sigma = [e/(R \times S_{electrode})]$, where e is the thickness of the pellet, R the measured resistance and $S_{electrode}$ the surface of the electrode (0.0346 cm^2).

The distribution of particle size was plot based on the direct measurement of 50 to 100 particles diameters from magnified SEM images.

3. Results and discussion

3.1 Calcination and crystallographic structure

The catalyst supports have to be crystalline enough to ensure a proper conductivity. It has been moreover reported in the literature that the rutile phase has to be favored [42]. Huang et al. [24] showed that the conductivity of the rutile phase of TiO_2:Nb was indeed six orders of magnitude higher than that of amorphous or anatase phases.

Amorphous materials, obtained after CO_2 supercritical drying, have thus to be calcined high enough in temperature to crystallize in the rutile phase. However, since the higher the calcination temperature, the lower the specific surface area, a compromise has to be found. To this end, our materials were calcined 5 h at different temperatures, between 500 and 800 °C, in flowing air or H_2/N_2.

A crystallographic analysis has first been performed on pure TiO_2 calcined at different temperatures in flowing air.

Details are provided as supplementary materials. Main conclusion is that no new oxide but TiO_2 is present for doped samples whereas small XRD peak shifts appear, what is representative of successful doping. The rutile phase only appears after calcination at temperature high enough (> 700°C) and the anatase to rutile transformation is delayed for Nb or Ta-doped TiO_2, not for V-doped TiO_2.

Since the presence of oxygen vacancies could increase the conductivity of the support [24] and also strongly affects the kinetic of phase transition [43], calcination in a reducing atmosphere was performed. Doped TiO_2 samples were prepared with 10 at.% Nb, Ta or V as a dopant and calcined for 5 h, at 800 °C, in flowing H_2/N_2.

Interestingly, such a treatment is highly beneficial to obtaining the rutile phase for all doped samples (Figure 1). Indeed, calcined at 800 °C in flowing H_2/N_2, all doped samples crystallized in the rutile phase. As mentioned, the phase transition rate is strongly influenced by the amount of oxygen vacancies, highly promoted in such calcination conditions. It can be concluded that calcination in a reducing atmosphere led to compensate the lack of oxygen vacancies resulting from Nb and Ta doping.

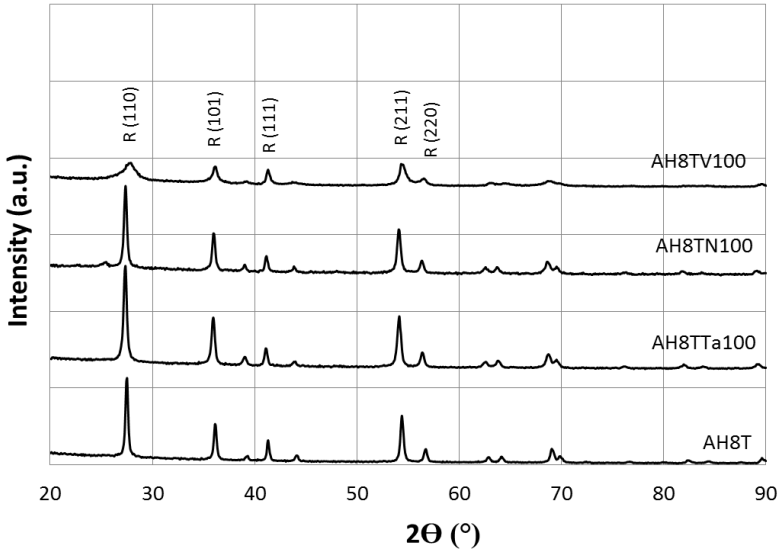

Figure 1. XRD of pure and doped TiO_2 aerogels calcined 5 h at 800 °C in flowing H_2/N_2 (5 vol.%)

A small peak shift is also observed on the main rutile peak (110). From 27.52° for undoped TiO_2 it is shifted to 27.37° for both Nb and Ta-doped TiO_2 and to 27.8° for V-doped TiO_2.

If the crystallinity looks similar for Nb and Ta-doped TiO_2, the V-doped sample exhibits much smaller crystallites evidenced from larger peak FWHM (full width at half maximum).

Looking at Figure 2 and the results obtained for different Nb levels, the niobium concentration should be limited to 5 at.% to avoid at maximum the presence of anatase. In our case and in agreement with Ruiz et al. [28], the limit of solubility of Nb in rutile TiO_2 stands between 5 and 10 at.%. This is confirmed by the stabilization of the shift (resulting from Nb insertion in the lattice) of the main rutile peak (110) from 10%. Above the limit of solubility in rutile (between 5 and 10%) Nb is stabilized in anatase in which solubility is higher (probably between 10 and 15% in our case as stated before). We can presume that increasing again the niobium level would result in the formation of niobium oxide.

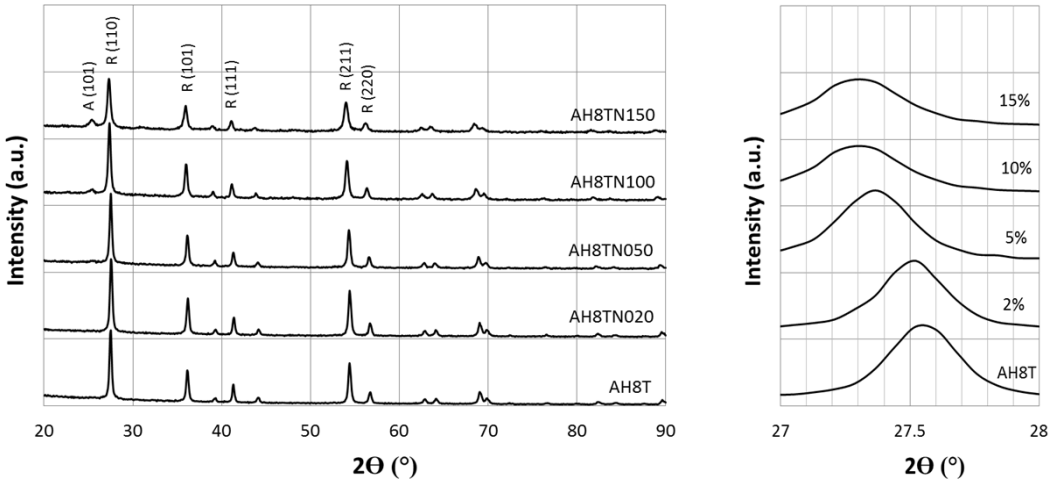

Figure 2. XRD of Nb-doped TiO_2 aerogels calcined 5 h at 800 °C in flowing H_2/N_2 (left) and R(110) peak shift (right) for different Nb contents.

Note that a different result was reported by Huang et al. [24] who obtained pure rutile after calcination at 800 °C in a reducing atmosphere with Nb concentration as high as 25 at.%.

In conclusion, to crystallize in the rutile structure, Nb or Ta-doped TiO_2 aerogels, prepared with the system selected in this study, have to be calcined at 800 °C in a reducing atmosphere (here 5 vol.% of H_2 in N_2). However, even in such conditions, too much a concentration of Nb leads to the presence of anatase.

The behavior of V-doped TiO_2 aerogel is different. Whatever the atmosphere of calcination V-doped TiO_2 samples all crystallize in rutile after calcination at 800°C. We can also conclude from our results that the presence of vanadium in the system facilitates the anatase to rutile phase transition.

3.2 Calcination and morphology

The calcination conditions and the presence of dopant are not only impacting the structure but also the morphology of TiO_2 aerogels which is of paramount importance for the foreseen application. It has thus been characterized with SEM and nitrogen sorption analysis with BET, BJH and t-plot data treatments.

The specific surface area of raw aerogels is relatively high, around 550 $m^2\ g^{-1}$ (Supplementary materials, figure 4).

Calcination in H_2/N_2 resulted in a tenfold increase of the specific surface area for pure TiO_2 compared to that of the same sample calcined in air (AH8T vs A8T, Figure 3 and supplementary materials), whereas both are in rutile phase.

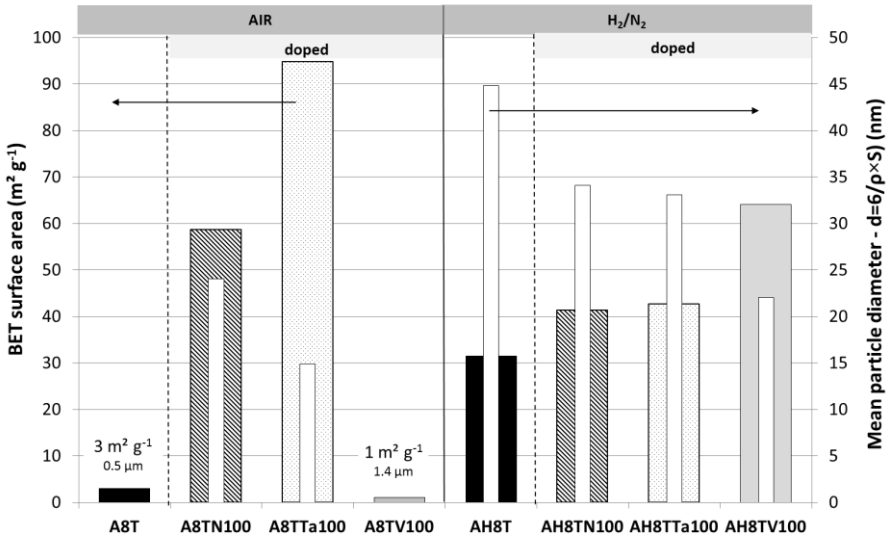

Figure 3. Specific surface area and mean particle diameter of pure and 10 at.% doped TiO_2 samples - Comparison between air and H_2/N_2 calcination atmosphere

Doping also resulted in an increase of the specific surface area of samples calcined in H_2/N_2. Even if more limited than after calcination in air it still keeps acceptable values close to 40 $m^2\ g^{-1}$ for 10 at.% Nb or Ta-doped samples. The evolution of the specific surface area of V-doped samples is noteworthy. Whereas it is very low after calcination in air (1 $m^2\ g^{-1}$), it is quite high after calcination in H_2/N_2 (65 $m^2\ g^{-1}$). Such specific surface areas are amongst the highest reported, in similar calcination conditions.

To complete the morphological characterization, SEM observations have been performed (Figure 4 and 5). The texture of TiO_2 aerogels, resulting from the agglomeration of roughly spherical particles, looks slightly dense. The apparent density is however difficult to measure since the monolithic nature was lost during supercritical drying and calcination. As expected, the particles' diameter increases with the calcination temperature. Starting from roughly 10 to 20 nm after calcination in air at 600 °C, the particles' diameter reaches values between 10 and 200 nm after calcination at 800 °C, larger particles being majority. In this case, the difference in diameter with that calculated from N_2 sorption results (500 nm) may be due to non-really spherical particles as shown on Figure 4 (A8T).

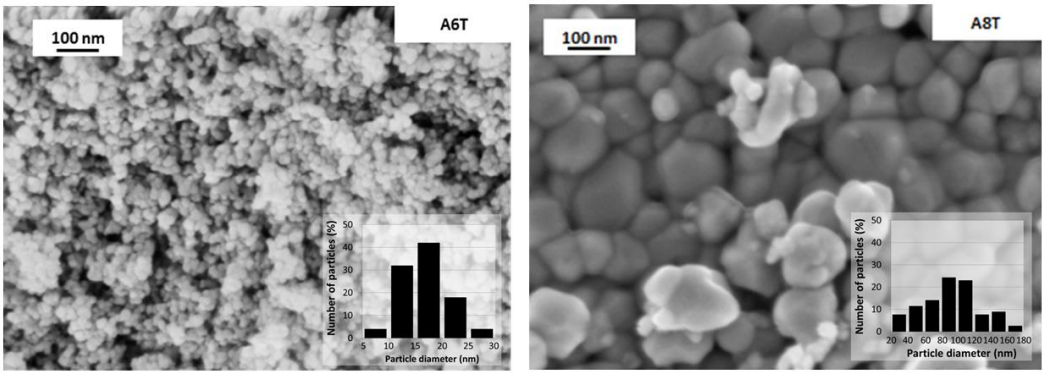

Figure 4. SEM images of TiO_2 aerogels calcined in air at 600 (A6T) and 800 °C (A8T) and distribution of particles size

Using a reducing atmosphere during the calcination results in a significant reduction of the particles' diameter for undoped TiO_2 (Figure 5), roughly from 100 nm to 40 nm.

Whatever the atmosphere of calcination, doping TiO_2 with Nb or Ta significantly decreases the particle size without changing their shape (Figure 5).

Nb has already been reported to inhibit grain growth [28, 44]. This was confirmed here both in oxidizing and reducing atmospheres. Particles are slightly larger in the latter case, in good agreement with N_2 sorption analysis (smaller specific surface area). A similar behavior was also observed with our Ta-doped aerogels.

On the contrary, doping with V results in much larger particles after calcination in air (about 1 µm in diameter!), which is also consistent with the very low specific surface area calculated from N_2 sorption analysis. In these calcination conditions, contrary to Nb or Ta, V also modifies notably the shape of grains which look more faceted. Particles are much smaller and more homogeneous in size after calcination in a reducing atmosphere.

Finally, all doped samples have similar mean particle diameter of about 20 to 25 nm after calcination in a reducing atmosphere, slightly smaller than that of pure TiO_2 (40 to 50 nm), in good agreement with N_2 sorption results.

The most drastic modification occurred for V-doped TiO_2 aerogel in accordance with N_2 sorption analysis and calculated specific surface areas. Their particles diameter decreased down to about 25 nm after calcination in H_2/N_2 from more than 1 µm after calcination in air.

If the specific surface area is a very important feature of catalyst supports, their pore size distribution is of major importance especially for fuel cell application. Indeed, it mainly governs the final morphology of the catalyst layer thus impacting fluids management and hence fuel cell performance. To be efficient in the foreseen application, a catalyst support has to present a very small micropore volume, large mesopores and some macropores to avoid flooding of the cathode catalyst layer at high current densities [39].

The determination of the pore size distribution is not that easy concerning aerogels. Some of them are known to be deformed during N_2 sorption analysis from intermediate relative pressure [45]. We made here the assumption that the calcination, at relatively high temperature, strengthens our aerogels enough to withstand the capillary forces applied during nitrogen sorption. Based on this assumption,

the pore size distribution, the pore volume and the micropore volume have been determined applying BJH and t-plot models on results obtained from N_2 sorption analysis.

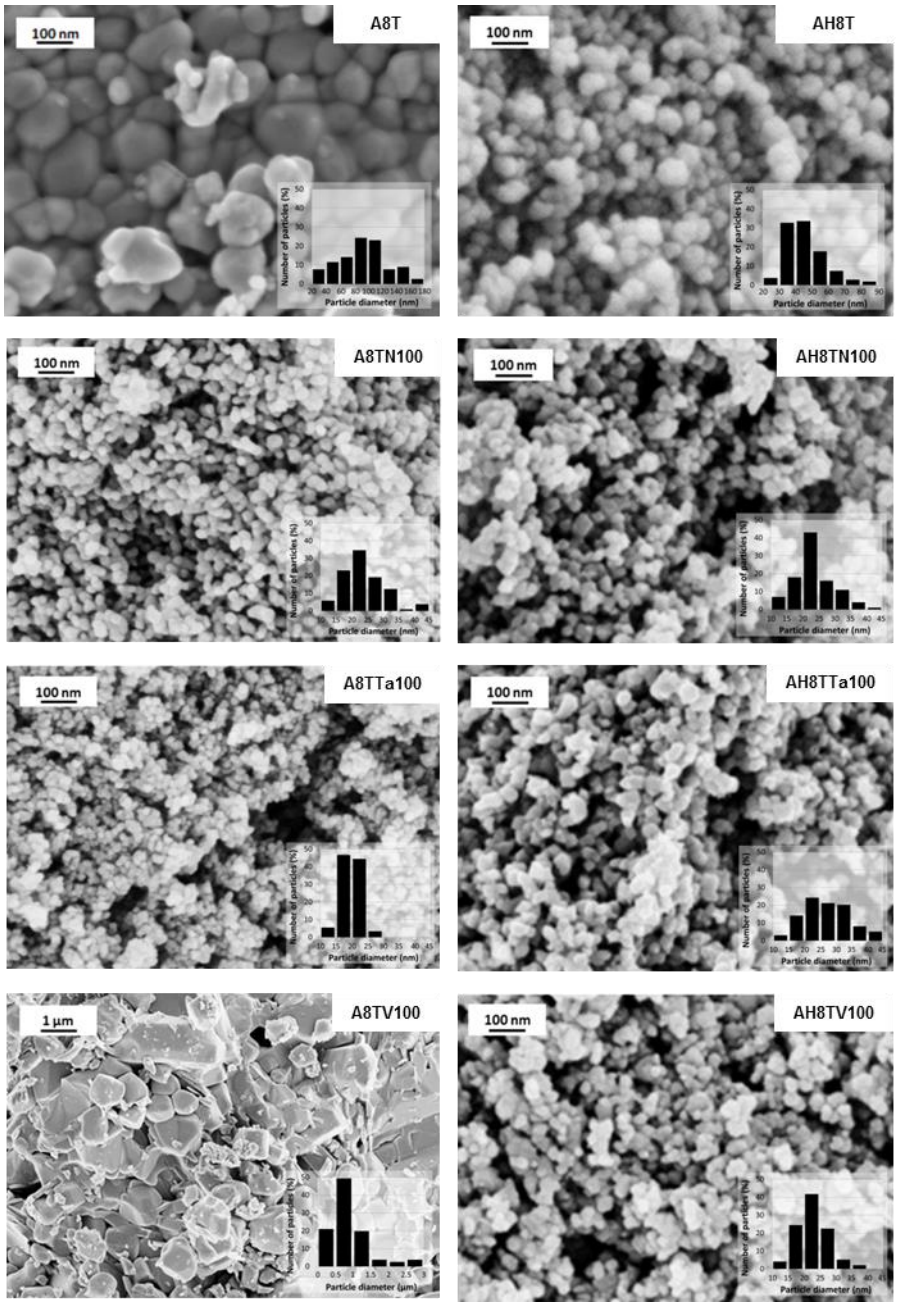

Figure 5. SEM images of pure and 10 at.% doped TiO_2 aerogels calcined 5 h at 800 °C in air (left) or H_2/N_2 (right) (N=Nb, Ta=Ta, V=V)

Table 1 gathers all the measured morphological features of the different aerogels samples analyzed.

Table 1. Morphological features of TiO_2 aerogels samples (S_{BET}= BET specific surface area, PSD_{BJH}= BJH Pore Size Distribution, V_PN_2 and $V_{P\mu}N_2$=pore and micropore volumes calculated from N_2 sorption)

Sample	Dopant	Atm. of calcination	S_{BET} ($m^2\ g^{-1}$)	PSD_{BJH} (nm)	V_PN_2 ($cm^3\ g^{-1}$)	$V_{P\mu}N_2$ ($cm^3\ g^{-1}$)
AT	No	Not calcined	546	25	3.4	$3\ 10^{-4}$
A5T	No	Air	149	14	0.8	-
A7T	No	Air	49	15	0.2	-
A8T	No	Air	3	29	0.024	$9\ 10^{-4}$
AH8T	No	H_2/N_2	32	18	0.15	$27\ 10^{-4}$
AH8TN100	Nb	H_2/N_2	44	18	0.24	$18\ 10^{-4}$
AH8TTa100	Ta	H_2/N_2	45	12;18	0.21	$48\ 10^{-4}$
AH8TV100	V	H_2/N_2	59	25	0.34	$15\ 10^{-4}$

The complete N_2 sorption isotherms performed on pure and doped TiO_2 aerogels are shown on figure 6. They are all representative of a classical mesoporous material: type-IV isotherm with a type-H1 hysteresis loop (according IUPAC classification) largely completed before P/P°=0.42. The shape of the hysteresis loops, with parallel adsorption and desorption branches, is consistent with SEM observations showing rather agglomeration of more or less spherical uniform particles. Adsorption and desorption branches are slightly less parallel for pure TiO_2 than for doped TiO_2, reflecting a wider distribution of particles size in agreement with SEM observation and particles size distribution (Figure 5). The plateau observed at large P/P° values, characteristic of type-IV isotherm, is less horizontal for doped samples probably due to a mix between type-II and type-IV isotherm. We may thus expect some macroporosity.

All samples present a narrow pore size distribution. AH8TTa100 apart, which presents significant contributions at 12 and 18 nm, it is almost monomodal for all materials, with an average pore diameter centered at 18 nm for pure and Nb or Ta-doped TiO_2 and 25 nm for V-doped TiO_2. A very small

contribution at larger pore diameters can be observed for doped samples, in agreement with the shape of the isotherm at large P/P° values discussed above (mix between type-II and type-IV isotherms). The pore size distribution is slightly broader for Nb and V-doped samples.

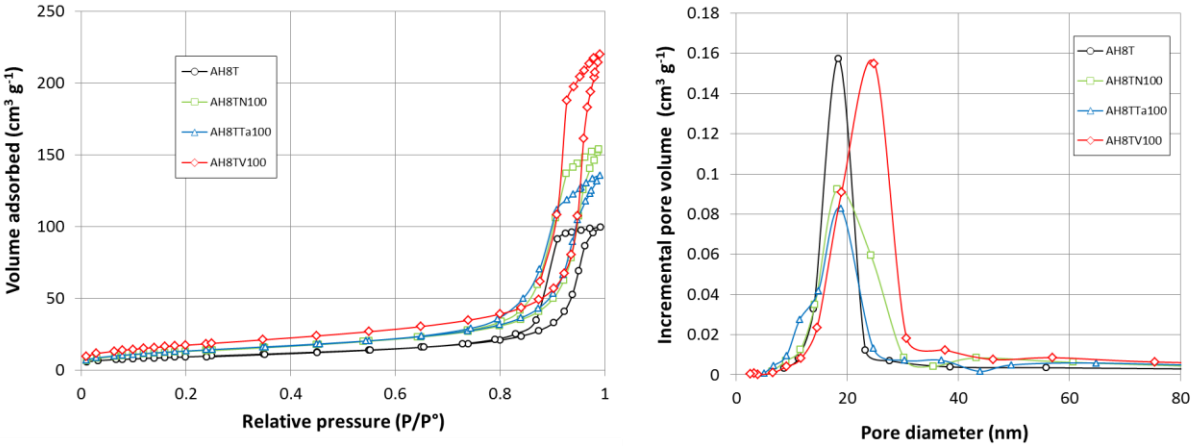

Figure 6. N_2 sorption isotherms (left) and pore size distribution (right) of pure and doped TiO_2 aerogels calcined in H_2/N_2 5 h at 800 °C.

The mesopore volume of TiO_2 aerogels decreased after calcination, whatever the atmosphere of calcination. Interestingly, a fivefold increase is observed for undoped TiO_2 calcined in a reducing atmosphere compared to calcination in air. Doping also leads to a slight increase in mesopore volume of the samples calcined in a reducing atmosphere (+ 60 or 40% resp. with 10 at.% of Nb or Ta and x2 with 10 at.% of V).

The micropore volume is increasing after calcination. However it is always negligible compared to the pore volume, roughly 3 to 4 orders of magnitude smaller. Note that, as reported by Siracusano et al. [25], doping TiO_2 with Ta results in a larger micropore volume than with Nb. No difference in micropore volume was observed between Nb and V doping.

After calcination at 800 °C in a reducing atmosphere, all the samples finally showed small particles (20 to 30 nm in diameter) exhibiting reasonable specific surface areas (30 to 60 $m^2\ g^{-1}$) while crystallizing in the rutile phase. Their micropore volume is negligible compared to the pore volume and their pore size distribution is centered between 15 and 30 nm.

Such a morphology is promising for the foreseen application. There is still room for optimization, especially concerning the pore size distribution where larger mesopores are expected along with some macropores.

3.3 Composition and dopant segregation

The conductivity is related to the crystallinity. It is moreover very much impacted by the doping level.

To confirm that the foreseen amount of dopant has really been introduced in the matrix, EDX and XPS analysis have been performed to determine respectively bulk and surface dopant concentration. Actually the doping level was calculated considering the respective atomic percentages of dopants and titanium obtained from EDX and XPS semi-quantitative analysis.

Whatever the dopant (Nb, Ta or V) and the synthesis atmosphere conditions (Air or H_2/N_2) of the doped TiO_2 samples, the calculated bulk levels (EDX) were very close to the expected values (Figure 7, plain markers). On the contrary, the dopant concentration is roughly two to four times higher on the surface (XPS) than in the bulk (Figure 7, open markers) reflecting some dopant segregation from the bulk to the surface. Such a phenomenon was already evidenced with HR-TEM and EDX by Akiyama et al. in the case of Nb [46]. It may be ascribed to different kinetics depending on the type of precursors used. Depending on the type of dopant and its concentration, such segregation, if it is stable, may favor or not the electronic conductivity.

It is noteworthy that the dopant segregation is more pronounced after calcination in air (Figure 7, squares), to a greater extent in the case of Nb and V doping, than after calcination in H_2/N_2 (Figure 7, circles). This may explain the slight difference in solubility observed and discussed previously.

In the case of Ta doping, the same type of segregation was observed but with little difference between oxidant and reducing calcination atmosphere. The difference in concentration between the bulk and the surface is also smaller than in the case of Nb or V.

Note that quite no segregation was observed for V doping after calcination in a reducing atmosphere.

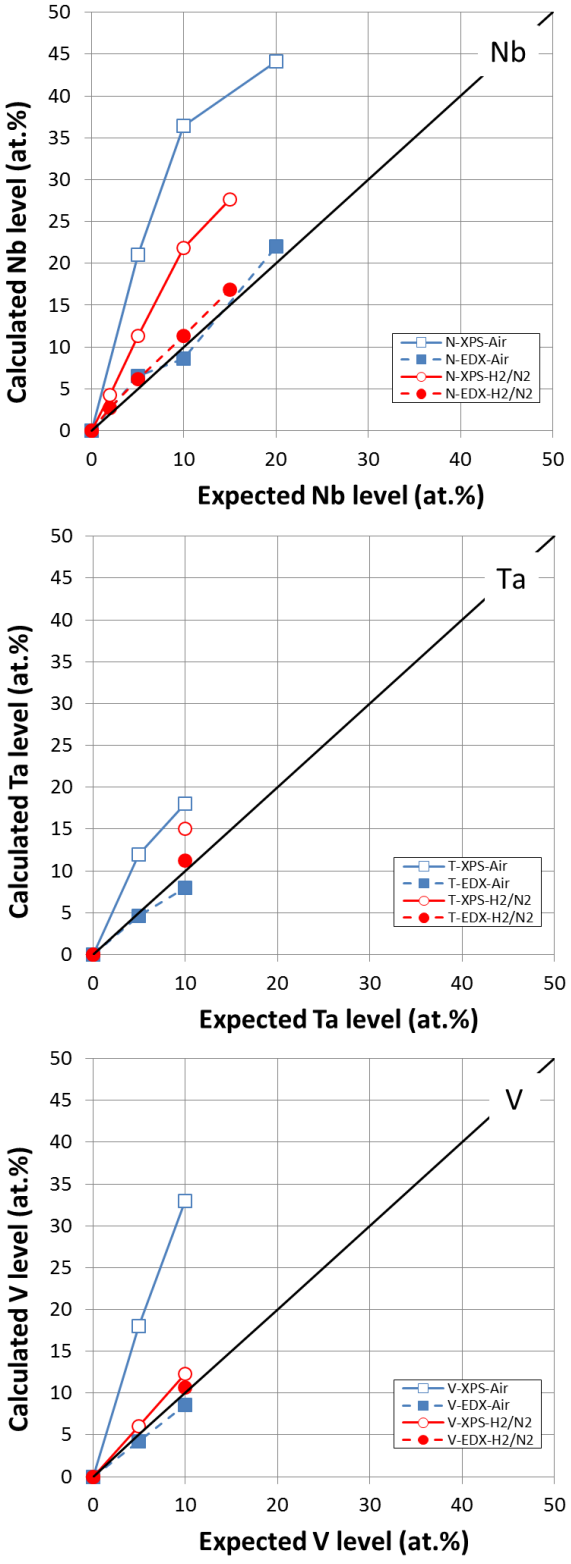

Figure 7. Comparison between expected and calculated doping levels from EDX (plain markers) and XPS (open markers) analysis – All samples calcined at 800°C in mentioned atmosphere (square: air, circles: H_2/N_2).

The Nb 10 at.% doped TiO_2 sample calcined at 800 °C in H_2/N_2 (AH8TN100) was observed by TEM. In order to perform EDX chemical analyses, this sample was also observed in scanning TEM (STEM) mode. Quantitative analysis was performed on EDX elemental maps in order to obtain the Ti and Nb at.% distribution across the TiO_2 grain. The Nb at% map (Figure 8.a) clearly revealed a higher concentration of Nb near the grain surface. The Nb segregation is also evidenced on the Ti and Nb at.% line profile extracted from the quantitative map (Figure 8.b). The Nb concentration near the surface is around 3 times higher than in the particle bulk in good agreement with previous results based on the comparison between SEM-EDX and XPS analysis. The thickness concerned with the segregation is roughly 4 nm in good agreement with XPS results as maximum intensity is coming out from the first nanometers.

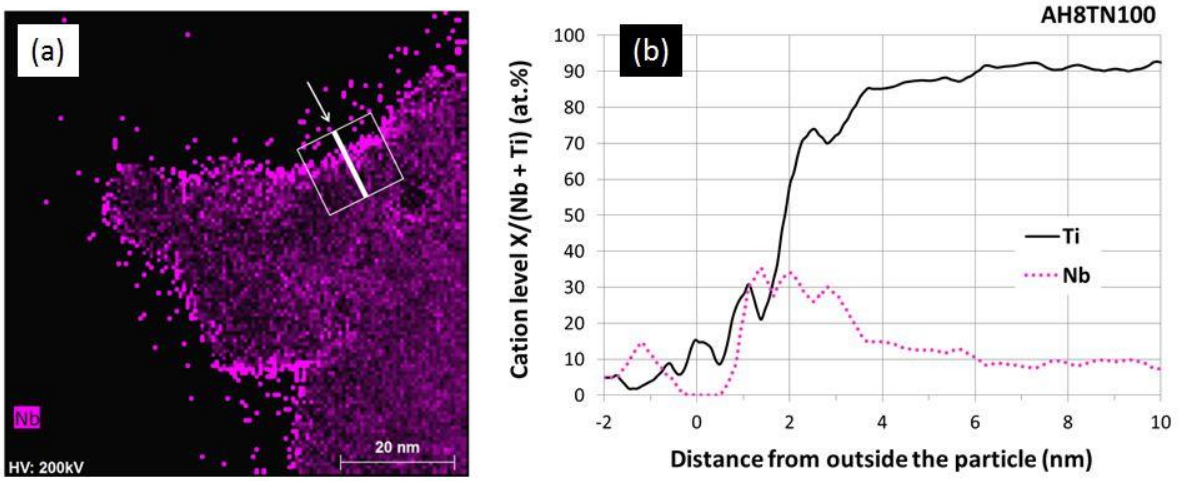

Figure 8. (a): Nb at.% quantitative elemental map across a grain of Nb-doped TiO_2 aerogel (AH8TN100) obtained from the EDX Ti and Nb elemental maps. – (b): line profile of Nb and Ti atomic concentration extracted from the quantitative map along the white line drawn on (a) and indicated by the arrow (in order to increase the signal/noise ratio, the signal was integrated in the square drawn on the figure along the line)

3.4 Electronic conductivity

In order to evaluate the influence of the different dopants on the TiO_2 electronic conductivity, it is preferable to limit at maximum the parasitic interface resistances. To this end the electronic conductivity was measured on xerogels. Xerogels indeed are much denser materials than aerogels, exhibiting much less grain boundaries. They were prepared by evaporative drying at room temperature during 2 days of gels synthesized following the protocol described in this paper. Similarly to aerogels, all xerogels were calcined in H_2/N_2 at 800 °C for 5 h. They all crystallized in the rutile phase, with a very low specific surface area, close to 1 m^2/g.

Electronic conductivities were measured by impedance spectroscopy at room temperature on pure and doped titania xerogel pellets (Figure 9) for Nb, Ta or V-doped TiO_2 (0.5, 2, 5, 10 and 15 at.%).

The pure TiO_2 xerogel (0 at.%) showed a very low electronic conductivity of about 10^{-6} S cm^{-1}.

All dopants have a beneficial impact on the electronic conductivity at different level of performance (Nb > Ta > V).

Whatever the dopant, the electronic conductivity is increasing with the dopant level, very significantly for Nb doping (4 to 5 orders of magnitude), less for Ta (3 orders of magnitude) and much less for V. Such differences may result from different i) induced point defects, ii) dopant distribution and segregation or even iii) sample densities.

The maximum value was obtained after doping at 10 at.% for Nb or Ta and at 5 at.% for V. Too high a dopant concentration results however in a decrease of electronic conductivity. A similar evolution of conductivity with the dopant level has already been reported for Nb-doped TiO_2 [47]. The best value was obtained for 10 at.% Nb-doped TiO_2 which reached a conductivity of about 0.08 S cm^{-1} (XH8TN100).

Measurements have also been carried out on aerogels calcined in a reducing atmosphere for comparison.

The conductivity of the pure aerogel calcined at 800 °C in a reducing atmosphere is one order of

magnitude lower than that of the pure TiO_2 xerogel calcined in the same conditions (0.07 10^{-6} $S.cm^{-1}$ vs 0.9 10^{-6} $S.cm^{-1}$).

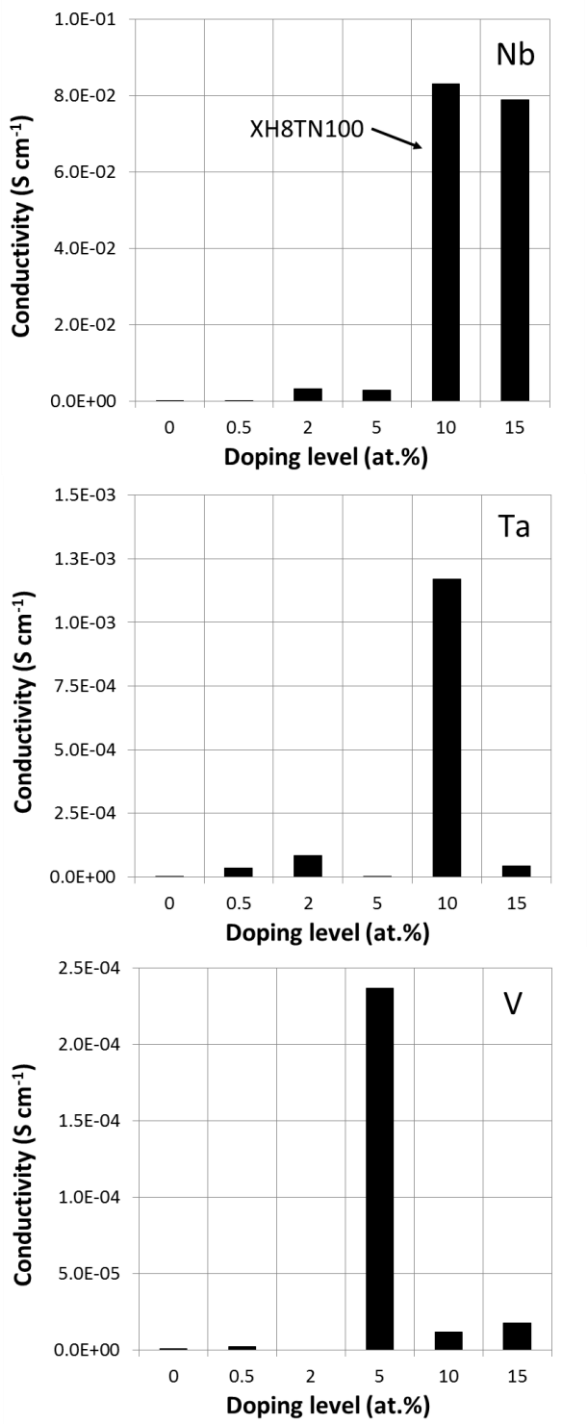

Figure 9. Evolution with the dopant level of the electronic conductivity of doped titania xerogel pellets calcined 5 h in H_2/N_2 at 800 °C.

The conductivity of 10 at.% Ta or Nb-doped aerogels remains very low (respectively 0.09 10^{-6} and 0.14 10^{-6} S cm^{-1}) compared to that of their xerogel counterparts.

The only significant increase of electronic conductivity (0.36 10^{-3} S cm^{-1}) was obtained after annealing the 10 at.% Nb-doped TiO_2 aerogel pellet in a reducing atmosphere, thus confirming, if necessary, the major importance of the particles connection. Actually, the electronic conductivity of individual particles is much probably increased after doping but the interface resistance between particles masks the advantage of doping.

Such low conductivities may limit the interest of these aerogels for the foreseen application. However, since PEMFC catalytic layers are very thin (several µm only) the number of grains boundaries across these layers is limited and so the contribution of the interface resistance to the total resistance.

Moreover, Pt nanoparticles subsequently deposited on the surface of the catalyst support will also narrow the depletion layer generated on the surface of semiconducting materials and favor electron conduction.

Nevertheless the morphology of our aerogels still needs to be improved to reduce interface resistances at maximium. In this context, we can expect large improvement from monolithic aerogels whose interconnected small particles will contribute to minimize internal resistances. We will now direct our work on the optimization of preparation of such monolithic materials.

4. Conclusion

The temperature and the atmosphere of calcination of our aerogels were found to impact the main features of the final catalyst support, i.e. their structure, morphology, composition and electronic conductivity.

Conditions which disadvantage the presence of oxygen vacancies (oxidizing atmosphere, hypervalent doping cations) delay the anatase to rutile phase transition. This was clearly evidenced comparing oxidizing and reducing atmospheres of calcination in the presence or not of Nb, Ta and V. The temperature of calcination is known to impact the morphology of powder materials (specific surface area, pore size distribution and particle size). It was also significantly impacted both by the atmosphere of calcination and doping. The presence of dopants (Nb, Ta or V) allowed to impressively increase the specific surface area of TiO_2 aerogels calcined in a reducing atmosphere. Such an

evolution is also related to the crystallographic phase, anatase being known to be stabilized for small particles.

Surface segregation was observed for all dopants, to different extent for Nb, V and Ta, depending on the atmosphere of calcination. It is always higher after calcination in air whatever the dopant (Nb, V or Ta).

Finally, the "bulk" electronic conductivity, measured on xerogels, was dramatically increased after doping and calcination in reducing atmosphere, the highest conductivity being obtained with Nb at 10 at.%.

Compared to classical carbon supports, the texture of aerogels can be optimized playing on the sol gel parameters. However their electronic conductivity remains for the moment too low compared to that of carbon regarding the foreseen application.

This first study on doped TiO_2 aerogels for PEMFC catalyst supports is paving the way towards their optimization. Considering the morphology of the aerogels obtained so far we believe that there is still room to improve the synthesis route playing on the sol-gel parameters in order to increase the specific surface area and to enlarge the pore size distribution. It may probably also impact the electronic conductivity. The overall performance of doped TiO_2 aerogels as catalyst support will have to be evaluated in real operating conditions. The thickness of the catalyst layer and the presence of deposited Pt nanoparticles are indeed impacting significantly the electron transfer across the electrode. This will be checked in a further study.

Acknowledgements

The authors gratefully acknowledge Pierre Ilbizian for supercritical drying, Gabriel Monge for XRD analysis and Suzanne Jacomet for SEM/EDX. This work was funded by the French National Research Agency PROGELEC programme, (ANR-12-PRGE-007 project SURICAT) and the European Union's Seventh Framework Program for the Fuel Cells and Hydrogen Joint Technology Initiative under grant agreement n325239 (FCH-JU project Nano-CAT). It was supported by Capenergies and Tenerrdis.

References

[1] R. Borup, J. Meyers, B. Pivovar, Chem. Rev. 107 (2007) 3904-3951

[2] E. Antolini, Appl. Catal. B-Environmental 88(1-2) (2009) 1-24.

[3] B.J. Eastwood, P.A. Christensen, R.D. Armstrong, N.R. Bates, J. Solid. State Electrochem. 3 (1999) 179-186

[4] S. Maass, F. Finsterwalder, G. Franck, R. Hartmann, C. Merten, J. of Power Sources 176(2) (2008) 444-451.

[5] H. Chhina, D. Susac, S. Campbel, O. Kesler, Electrochem. Solid State Lett. 12 (2009) B 97-B100

[6] X. Wang, W. Li, Z. Chen, M. Waje, Y. Yan, J. Power Sources 158 (2006) 154-159

[7] K. Yasuda, A. Taniguchi, T. Akita, T. Iroi, Z. Siroma, Phys. Chem. Chem. Phys. 8(6) (2006) 746-752.

[8] K. Sasaki, F. Takasaki, Z. Noda, S. Hayashi, Y. Shiratori, K. Ito, ECS Trans. 33(1) (2010) 473-482

[9] B. O'Regan, M. Grätzel, Nature 353 (1991) 737 - 740

[10] M. Grätzel, J. of Photochemistry and Photobiology C: Photochemistry Rev. 4 (2003) 145–153

[11] A. Fujishima, K. Honda, Nature 238 (1972) 37-38

[12] J. Nowotny, T. Bak, M.K. Nowotny, L.R. Sheppard, Int. J.of Hydrogen Energy 32 (2007) 2609-2629

[13] L. Znaidi, R. Seraphimova, J.F. Bocquet, C. Colbeau-Justin, C. Pommier, Mater. Research Bull. 36 (2001) 811–825

[14] T. Kasuga, M. Hiramatsu, A. Hoson, T. Sekino, K. Niihara, Langmuir 14 (1998) 3160-3163

[15] G.K. Mor, O.K. Varghese, M. Paulose, K. Shankar, C.A. Grimes, Solar Energy Mater. and Solar Cells 90 (2006) 2011-2075

[16] D. Kowalskia, D. Kimb, P. Schmuki, Nano Today 8 (2013) 235—264

[17] Y. Suzuki, B. Pichon, D. D'Elia, C. Beauger, S. Yoshikawa, J. of the Ceram. Soc. of Japan 117 (2009) 381-394

[18] M. Schneider, A. Baiker, J. Mater. Chem. 2(6) (1992) 587-589

[19] J.J. Pietron, A.M. Stux, R.S. Compton, D.R. Rolison, Solar Energy Mater. & Solar Cells 91 (2007) 1066–1074

[20] S. Boujday, F. Wünsch, P. Portes, J.-F. Bocquet, C. Colbeau-Justin, Solar Energy Mater. and Solar Cells 83 (2004) 421-433

[21] Y. Suzuki, M.-H. Berger, D. D'Elia, P. Ilbizian, C. Beauger, A. Rigacci, J.-F. Hochepied, P. Achard, Nano 3(4) (2008) 1-7

[22] D. D'Elia, C. Beauger, J.-F. Hochepied, A. Rigacci, M.-H. Berger, N. Keller, V. Keller-Spitzer, Y. Suzuki, J.-C. Valmalette, M. Benabdesselam, P. Achard, Int. J. of Hydrogen Energy 36 (2011) 14360-14373

[23] M. Popa, D. Macovei, E. Indrea, I. Mercioniu, I.C. Popescu, V. Danciu, Microporous and Mesoporous Materials 132 (2010) 80–86

[24] S.Y. Huang, P. Ganesan and B.N. Popov, Appl. Catal. B: Environmental 96 (2010) 224-231

[25] S. Siracusano, A. Stassi, E. Modica, V. Baglio, A.S. Arico, Int. J. of Hydrogen Energy 38 (2013) 11600-11608

[26] D. Morris, Y. Dou, J. Rebane, C.E.J. Mitchell, R.G. Egdell, Physical rev. B 61(20) (2000) 13445-13457

[27] L.R. Sheppard, T. Bak, J. Nowotny, J. Phys. Chem. B 110 (2006) 22447-22454

[28] A.M. Ruiz, G. Dezanneau, J. Arbiol, A. Cornet, J.R. Morante, Chem. Mater. 16 (2004) 862-871

[29] L.A. Balagurov, I.V. Kulemanov, A.F. Orlov, E.A. Petrova, Russian microelectronics 41(8) (2012) 503-507

[30] M. Bettinelli, V. Dallacasa, D. Falcomer, P. Fornasiero, V. Gombac, T. Montini, L. Romano, A. Speghini, J. of Hazard. Mater. 146 (2007) 529-534

[31] K.W. Park, K.S. Seol, Electrochem. Comm. 9 (2007) 2256-2260

[32] S.Y. Huang, P. Ganesan, B.N. Popov, Appl. Catal. B: Environmental 102 (2011) 71-77

[33] L. Chevalier, A. Bauer, S. Cavaliere, R. Hui, J. Rozière, D. Jones, Appl. Mater. and Interfaces 4 (2012) 1752-1759

[34] A. Bauer, L. Chevalier, R. Hui, S. Cavaliere, J. Zhang, D. Jones, J. Rozière, Electrochimica Acta 77 (2012) 1-7

[35] I. Savych, J. Bernard d'Arbigny, S. Subianto, S. Cavaliere, D.J. Jones, J. Rozière, J. of Power Sources 257 (2014) 147-155

[36] A. Smirnova, X. Dong, H. Hara, A. Vasiliev, N. Sammes, Int. J. of Hydrogen Energy 30(2) (2005) 149-58.

[37] M. Ouattara-Brigaudet, S. Berthon-Fabry, C. Beauger, M. Chatenet, N. Job, M. Senmour, P. Achard, Int. J. of Hydrogen Energy 37 (2012) 9742-9757

[38] M. Ouattara-Brigaudet, S. Berthon-Fabry, C. Beauger, P. Achard, Int. J. of Hydrogen Energy 39 (2014) 1420-1429

[39] M. Ouattara-Brigaudet, C. Beauger, S. Berthon-Fabry, P. Achard, Fuel Cells 11(6) (2011) 726-734

[40] N. Hüsing, U. Schubert, Angew. Chem. Int. Ed. 37 (1998) 22-45

[41] Handbook of chemistry and physics, 66th edition, CRC Press (1985) B-155

[42] J.H. Kim, A. Ishihara, S. Mitsushima, N. Kamiya, K.I. Ota, Electrochim. Acta 52 (2007) 2492-2497

[43] D.A.H. Hanaor, C.C. Sorrell, J. of Mater. Sci. 46(4) (2011) 855-74.

[44] R.F. Chen, L. Zhang, Y. Wei, D.L. Hou, J. Mater. Sci. 42(17) (2007) 7141-7146

[45] G.W. Scherer, M.S. Douglas, D. Stein, J. of Non-Crystalline Solids 186 (1995) 309-315

[46] K. Akiyama, N. Toyama, K. Muroaka, M. Tsunashima, J. Am. Ceram. Soc. 81 (1998) 1071-1073

[47] Y. Liu, J.M. Szeifert, J.M. Feckl, B. Mandlmeier, J. Rathousky, O. Hayden, D. Fattakhova-Rohlfing, T. Bein, ACS Nano 4(9) (2010) 5373-5381

Supplementary materials

Crystallographic analysis of pure and doped TiO_2 calcined in air

XRD peak intensity ratios were used in order to quantify the degree of the anatase to rutile phase transformation after calcination at 800 °C in air, using the empirical relationship [1].

$$R(T) = 0.679\times[I_R/(I_R+I_A)] + 0.312\times[I_R/(I_R+I_A)]^2 \qquad \text{Eq. 1}$$

where R(T) is the content of rutile after calcination at T in °C, I_A is the intensity of the main anatase peak at 2Θ = 25.3 ° (101), and I_R is the intensity of the main rutile peak at 2Θ = 27.44 ° (110).

As expected, the higher the calcination temperature the better the crystallinity of TiO_2 (Figure 1).

If after calcination at 600 °C only anatase could be detected (A6T) as confirmed by the absence of the most intense peak of rutile at 2 Θ = 27.44 ° (R 1 1 0), rutile is by far the major phase detected after calcination at 800 °C, with only 2% of anatase. So, consistently with Campbell et al. [2], in flowing air the anatase to rutile phase transformation occurs between 600 and 800 °C for our pure TiO_2 aerogels.

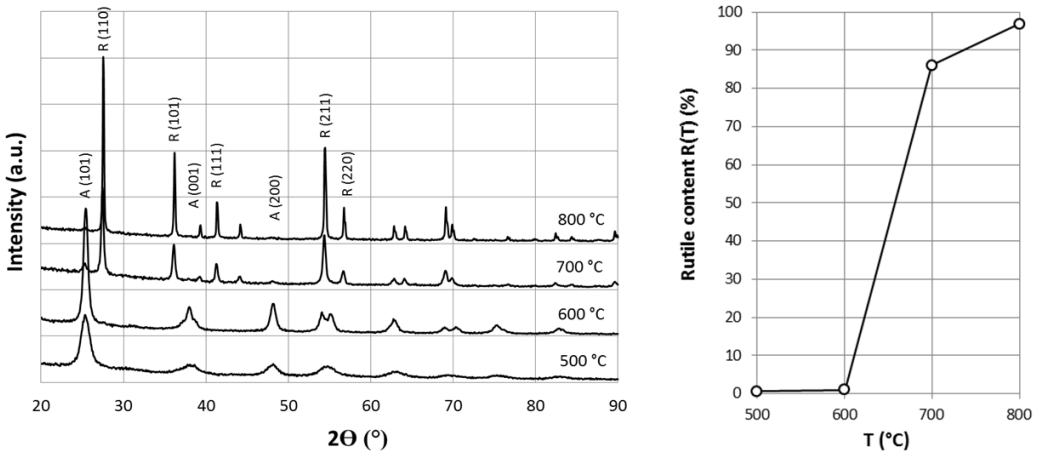

Figure 1. XRD of TiO_2 aerogels calcined in flowing air, 5 h at 500 °C, 600 °C, 700 °C and 800 °C (left) and rutile content (right)

Whatever the dopant, Nb, V or Ta, at 10 at.% doping level, no other oxide but TiO_2 could be detected in all doped TiO_2 samples, what is a good indication for a successful doping (Figure 2). Additionally, a

small peak shift was observed for Nb or Ta-doped TiO_2. Whereas the main anatase peak (101) is positioned at 25.47° for undoped TiO_2, it is shifted to 25.31° for both Nb or Ta-doped TiO_2, resulting from an expansion of the lattice after doping, in agreement with the respective diameter of Ti^{4+} (0.61 Å) and Nb^{5+} (0.64 Å) cations. It is clear from figure 2 that doping TiO_2 with niobium delays the anatase to rutile phase transition as reported by Arbiol at al. [3]. Indeed, large amount of anatase is still present in Nb-doped TiO_2 (10 at.%) even after calcination for 5 h in Air at 800 °C. The delay in the phase transition may be related to the limit of solubility of the dopant in the metal oxide matrix as reported by Ruiz et al. [4] (6 and 10 at.% for Nb respectively in rutile and anatase). We observed a similar phase transition delay for Ta-doped TiO_2. On the contrary, vanadium has no influence on the phase transition.

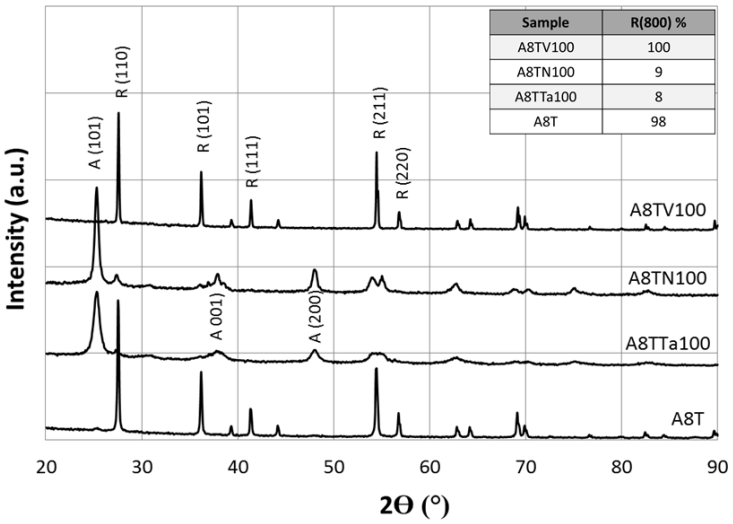

Figure 2. XRD of doped TiO_2 aerogels calcined in flowing air, 5 h at 800 °C and rutile content (table)

From our calculations, doping with 10 at.% of Nb or Ta led only to about 10% of rutile after calcination in air at 800 °C.

The phenomenon is actually related to the concentration of oxygen vacancies which govern the anatase to rutile phase transition and depends on the dopant [5]. Oxygen vacancies are natively present in TiO_2. Their concentration depends on the oxygen partial pressure according to equilibrium:

$$O_o = ½\ O_2 + Vo^{\circ\circ} + 2\ e' \qquad \text{Eq. 2}$$

where O_O stands for oxygen in oxygen crystallographic site, O_2 for gaseous oxygen, $V_O^{\circ\circ}$ for oxygen vacancy and e' for electron.

Substituting Ti^{4+} with Nb^{5+} or Ta^{5+} during doping results in the creation of positively charged point defects, Nb_{Ti}° or Ta_{Ti}°, resulting in a decrease of the concentration of oxygen vacancies by charge compensation effect as already reported in the case of Nb doping [5, 6]. Such a decrease finally impacts the anatase to rutile phase transition during calcination in air even at 800 °C for 5h.

The absence of anatase after vanadium doping means that the oxygen vacancies concentration is not reduced after doping. Vanadium may either not have been included in the TiO_2 lattice or in its 4^+, nay 3^+, oxidation state, so without any impact, or a beneficial one, on the concentration of oxygen vacancies. This would be consistent with numerous stable oxidation states known for vanadium. The presence of vanadium is even beneficial to the phase transition since no anatase is present in the V-doped TiO_2 sample whereas 2% were detected in the pure TiO_2 sample calcined in the same conditions.

We have then checked the influence of the Nb content on the anatase to rutile phase transition.

As expected, the amount of rutile with respect to that of anatase is decreasing with the increase of Nb in the matrix, between 0 and 10 at.% in our case (see the evolution of the rutile content in Figure 3). Note that in similar conditions, Ruiz et al. [4] obtained anatase for Nb content higher than 6 at.%. Here, only 14 % of rutile is present after 5 at% of Nb. This doping level is close to the limit of solubility determined by Ruiz et al. The segregation discussed later may be responsible of higher Nb concentration on surface which could account for the presence of anatase in this sample. At higher Nb content, i.e. from 15 at.% and above, the rutile content increases, almost up to 30% for 20 at.% of Nb. It is noteworthy that Nb oxide can also be detected from 15 at.% and above. Ruiz et al. [4] observed the same phenomenon for Nb levels higher than 8 at.%, i.e. above the limit of solubility they determined for rutile. The niobium oxide was identified to be $TiNb_2O_7$. So, in agreement with Ruiz et al. [4] the limit of solubility in anatase, above which niobium oxide appears, would also be here between 10 and 15%.

Such an evolution may be related to the oxidation state of Nb, be it 5^+ or 3^+, as well as to the presence of niobium oxide at relatively high Nb contents. In its 5^+ oxidation state, Nb leads to the formation of

positively charged point defects Nb_{Ti}°, whereas in its 3^{+} oxidation state, it leads to the formation of negatively charged point defects $Nb_{Ti}^{'}$. The former will contribute to a decrease of the oxygen vacancies concentration, through charge compensation effect, while the latter will have an opposite impact. Assuming that, just like for antimony in tin oxides [7, 8], Nb^{5+} is stabilized only at low levels while Nb^{3+} is the stable species at higher Nb content would account for the observed evolution of the rutile content in the calcined products. Rutile begins to decrease with respect to anatase due to the presence of Nb_{Ti}°, major defect till 10 at.% and its impact on the $V_O^{\circ\circ}$ concentration. At 15 at.%, the stabilization of Nb^{3+} ($Nb_{Ti}^{'}$) would make the oxygen vacancies concentration increase, thus facilitating the anatase to rutile phase transition. Hence, the rutile content increases again.

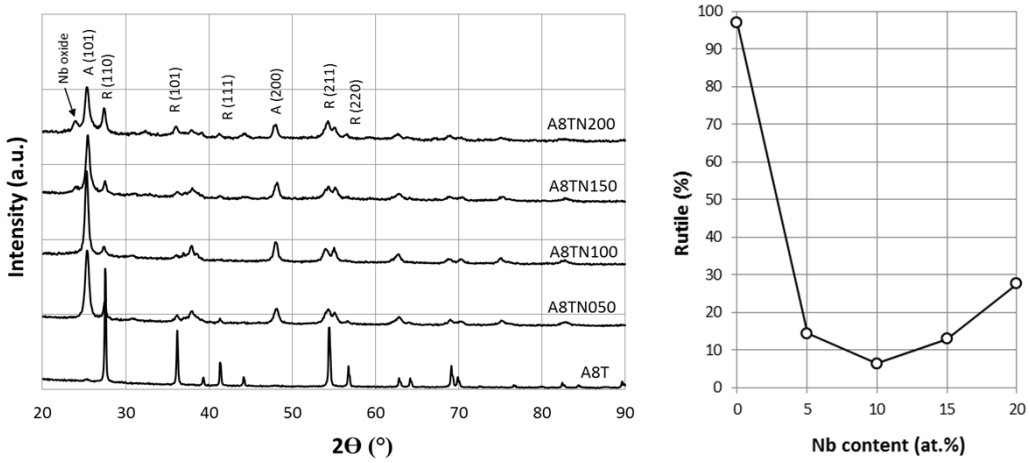

Figure 3. XRD of Nb doped TiO_2 aerogels calcined in flowing air, 5 h at 800 °C (left) and evolution of rutile content vs Nb doping level (right)

N2 sorption on pure and doped TiO_2 calcined in air

The specific surface area of raw aerogels is relatively high, around 550 $m^2 g^{-1}$ (Figure 4). As expected, it is lower for all calcined samples, the higher the calcination temperature the lower the specific surface area. It decreased down to 3 $m^2 g^{-1}$ after calcination at 800°C in air.

Doping with Nb and Ta (Figure 5) results in a very large increase of the specific surface area of the samples calcined in air at 800 °C (x20 for Nb and x30 for Ta). The dopant level does not have any significant influence on the specific surface area.

Note that all V-doped TiO_2 samples kept a very small specific surface area after calcination in air (1 $m^2 g^{-1}$).

The increase of the specific surface area after doping is probably related to the stabilization of the anatase phase for Nb and Ta-doped samples while undoped and V-doped samples crystalized in rutile phase, usually resulting in larger particles (article Figure 2).

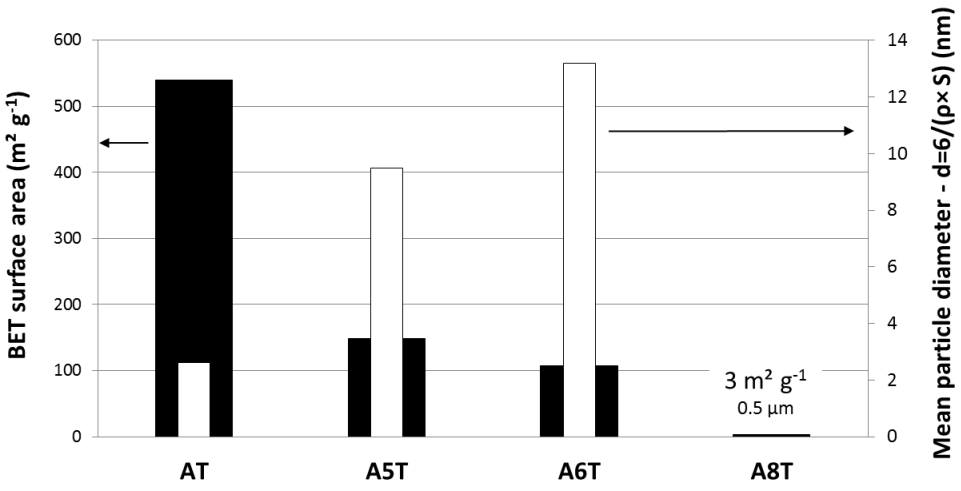

Figure 4. Specific surface area and mean particle diameter of pure aerogel TiO_2 samples, as a function of the calcination temperature in air (AT: raw aerogel, A5T: 500 °C, A6T: 600 °C, A8T: 800 °C).

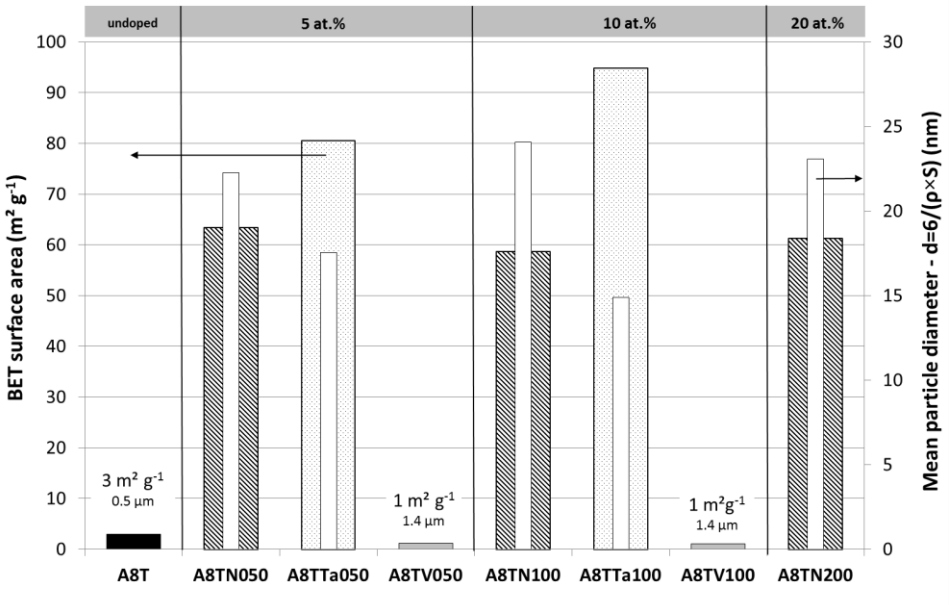

Figure 5. Specific surface area and mean particle diameter of pure and doped TiO_2 samples calcined 5 h at 800 °C in air

References

[1] L.E. Depero, L. Sangaletti, B. Allieri, E. Bontempi, R. Salari, M. Zocchi, C. Casale, M. Notaro, J. of Mater. Research 13(6) (1998) 1644-9.

[2] L.K. Campbell, B.K. Na, E.I. Ko, Chem. Mater. 4(6) (1992) 1329-33.

[3] J. Arbiol, J. Cerda, G. Dezanneau, A. Cirera, F. Peiro, A. Cornet, J.R. Morante, J. of Appl. Phys. 92(2) (2002) 853-61

[4] A.M. Ruiz, G. Dezanneau, J. Arbiol, A. Cornet, J.R. Morante, Chem. Mater. 16 (2004) 862-871

[5] M.K. Akhtar, S.E. Pratsinis, J. Am. Ceram. Soc. 75 (1992) 3408

[6] M.C. Carotta, M. Ferroni, D. Gnani, V. Guidi, M. Merli, G. Martinelli, M.C. Casale, M. Notaro, Sens. Actuators B-Chemical 58 (1999) 310-317

[7] M. Caldararu, M.F. Thomas, J. Bland, D. Spranceana, Appl .Catal. a-General 209(1-2) (2001) 383-390.

[8] G. Ozouf, C. Beauger, J. of Mater. Sci., 51(11) (2016) 5305-5320